

A Beam-Driven Proton Irradiation Setup for Precision Radiation Damage Tests of Silicon Detectors

Pascal Wolf^{a,*}, Dennis Sauerland^b, Reinhard Beck^b, Jochen Dingfelder^a

^aPhysikalisches Institut (PI), Rheinische Friedrich-Wilhelms-Universität Bonn, Nußallee 12, 53115 Bonn, Germany

^bHelmholtz Institut für Strahlen- und Kernphysik (HISKP), Rheinische Friedrich-Wilhelms-Universität Bonn, Nußallee 14-16, 53115 Bonn, Germany

Abstract

A proton irradiation site for silicon detectors has been developed and commissioned at the Bonn Isochronous Cyclotron. The accelerator provides 14 MeV proton beams of up to 1 μA at beam widths of a few mm to the setup. Devices Under Test (DUTs) are irradiated inside a cooled, thermally-insulated box at $\leq -20^\circ\text{C}$, while being moved through the beam in a row-based scan pattern to achieve uniform fluence distributions. Custom-made diagnostics allow for beam-based, on- and offline dosimetry, enabling a beam-driven irradiation routine which produces uniform fluence distributions with standard deviations $\ll 1\%$. Dedicated irradiations of thin titanium foils are performed to compare the commonly-used dosimetry via metallic foil activation to the beam-based approach. Within the error margins, both methods are in agreement, whereas the beam-based technique yields lower uncertainties of typically $\leq 2\%$. Simulations indicate a reduction of the initial proton energy to (12.28 ± 0.06) MeV on the DUT. Characterization of six 150 μm -thin, passive LFoundry sensors before and after irradiation yield a proton hardness factor of $\kappa_p = 3.71 \pm 0.11$, which is in agreement with expectations, allowing to irradiate up to $10^{16} n_{\text{eq}} \text{cm}^{-2}$ within a few hours.

Keywords: irradiation, silicon detector, NIEL damage, beam monitoring

1. Irradiation Site

1.1. Setup

The irradiation site is located at the Bonn Isochronous Cyclotron which typically provides light ions up to alpha particles between 7 MeV to 14 MeV per nucleon. Commonly, the accelerator delivers a 13.6 MeV (≈ 12.3 MeV on DUT) proton beam with currents between 20 nA to 1 μA and widths of a few mm Full Width Half Maximum (FWHM) to the site. The setup is depicted in fig. 1. The beam passes through a calibrated beam monitor into a thermally-insulated cool box, mounted on a *scan stage* consisting of two linear stages. The scan stage is installed on a retractable table, allowing a Faraday Cup (FC) on a linear stage to be driven in front of the beam monitor for calibration, replacing the cool box.

1.2. Devices Under Test

Typical DUTs arrive at the site on a carrier Printed Circuit Board (PCB) or Single Chip Card (SCC). They

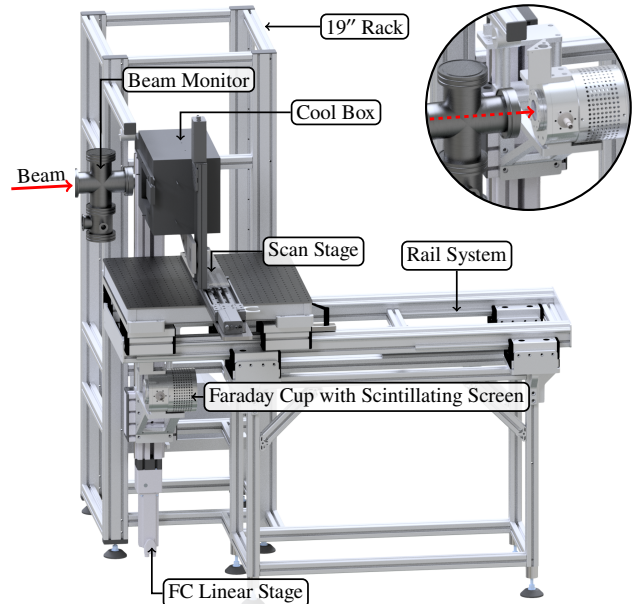


Figure 1: CAD render of the setup, adapted from [1]. Upper right shows the calibration configuration.

*Corresponding author

Email address: wolf@physik.uni-bonn.de (Pascal Wolf)

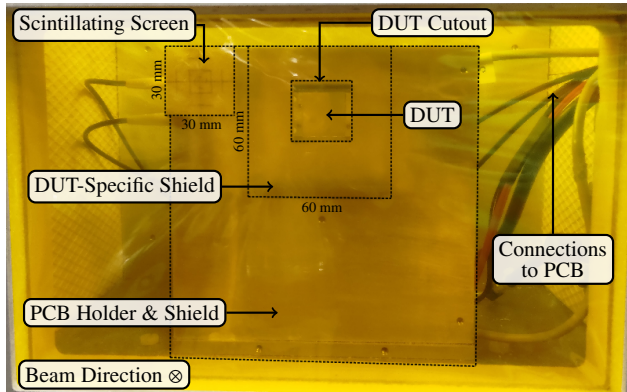


Figure 2: Front view of cool box with an installed carrier PCB, exposing only the DUT to the beam.

are mounted behind a 6 mm-thick Al-shield inside the cool box. A front view of the box through its Kapton entrance window is shown in fig. 2. The shield is composed of a generic sample holder as well as a DUT-specific, in-house manufactured cut-out, exposing only the silicon to the beam. On the top-left of the shield, a scintillating screen is located, enabling beam-based alignment of the setup and serving as the origin position of the irradiation routine. A feed-through allows to connect power and readout cables to the DUT during irradiation. Other DUTs not situated on carrier PCBs, such as bare sensors and diodes, are irradiated on a dedicated carrier plate. During irradiation, the box is continuously flushed with nitrogen gas, cooled by a liquid nitrogen heat exchanger, maintaining temperatures of $\leq -20^\circ\text{C}$ to prevent annealing and a dry atmosphere to avoid condensation.

2. Beam Monitoring

2.1. Principle

The beam diagnostics are based on the effect of Secondary Electron Emission (SEE) on the surface of materials penetrated by fast ions as described in [2]. The ratio of emitted electrons per initial ion is called Secondary Electron Yield (SEY) γ and can be defined using the SEE as well as ion beam current as

$$\gamma = \frac{I_{\text{SEE}}}{I_{\text{beam}}} \cdot z_{\text{ion}}, \quad (1)$$

where z_{ion} is the number of elementary charges q_e carried by the ion. Generally, I_{SEE} depends on a variety of parameters such as pressure, target temperature, ion type and energy as well as beam intensity [2]. Assuming a monoenergetic proton beam inside a vacuum, γ

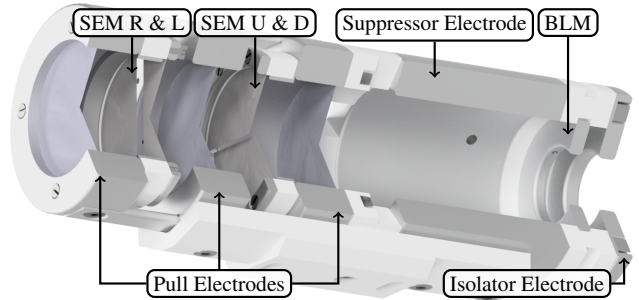


Figure 3: CAD render of the custom-made beam monitor from [1]. The beam passes from left to right.

is approximately constant over orders of magnitude of beam intensity and eq. (1) yields a constant. Allowing the beam to penetrate a thin foil enables online beam monitoring by one-time determination of γ and subsequent, continuous measurement of I_{SEE} .

2.2. Custom Monitor

Building on this principle, a custom beam monitor concept was developed and is depicted in fig. 3. It consists of a Secondary Electron Monitor (SEM) as well as a Beam Loss Monitor (BLM) module for beam current and position as well as beam loss monitoring. The SEM is composed of two, carbon-coated (≥ 70 nm, to anticipate carbon build-up due to irradiation [3] and subsequent change of SEY), $4.5 \mu\text{m}$ Al-foil pairs, segmented in the vertical (SEM L+R) and horizontal plane (SEM U+D). Al-foil pull electrodes are placed in between at 100 V, removing Secondary Electrons (SEs) from the SEM foils. Subsequently, the individual SEE currents of each respective SEM foil I_{SEE} (L|R|U|D) can be measured. The BLM module consists of a 3 mm-thick Al-iris enclosed by a suppressor as well as isolator electrode at -100 V and functions as an internal FC, allowing to detect beam cut-off. The SEM currents in combination with a beam current measurement via an external FC, as shown in fig. 1, can be used to calibrate the beam monitor according to eq. (1). This is depicted for protons in fig. 4, where $\gamma = (21.64 \pm 0.06)\%$ over approximately an order of magnitude of beam current. The current signals of the beam diagnostics are converted to voltages using a custom, analog readout board. It features a transimpedance amplifier chain for each signal channel with variable input current scales, allowing to adapt to different signal amplitudes. The resulting voltages are mapped to $\pm 5\text{V}$ and digitized using an Analog-to-Digital Converter (ADC) board. The relative uncertainty of the readout chain is in the order of 2%. More

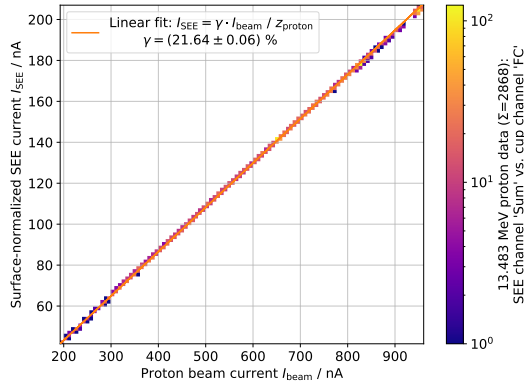


Figure 4: Beam monitor calibration for 13.483 MeV protons.

detailed description of the diagnostics can be found in [1, 4].

3. Irradiation Procedure

3.1. Preparation

A beam monitor calibration is performed prior to each irradiation to compensate systematic errors due to run-by-run variations in ion energy and environmental parameters. Moreover, a maximum estimate of the horizontal and vertical beam FWHM is made from visual inspection on the scintillating screen on the FC with a camera, to account for them in the irradiation routine. The DUT is installed in the cool box and cooled to $\leq -20^\circ\text{C}$. Subsequently, the setup is aligned by simultaneously centering the beam spot in the beam monitor as well as on the scintillation screen of the cool box, using a camera, defining the origin position for the irradiation.

3.2. Routine

The irradiation routine is shown schematically in fig. 5. In reference to the origin position, a grid with equidistantly-spaced rows is generated, using the DUT's position and cross section, on which it is moved through the stationary beam. The assembled grid covers an area larger than the DUT cross section to include margins considering the beam FWHM as well as the required acceleration distance to reach the scan velocity v_{scan} . Choosing a row separation $\Delta y \ll \text{FWHM}$ and ensuring a constant velocity when traversing the DUT, results in the integration of the beam profile along the respective dimensions, producing a uniform fluence distribution around the DUT as indicated in fig. 5. The

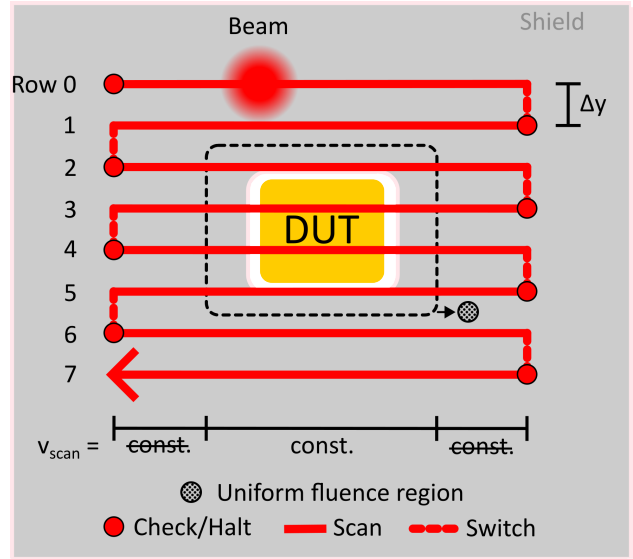


Figure 5: Irradiation pattern. Beam parameters are checked prior to scanning each row

traversal of all rows of the grid constitutes a *complete scan*. After completing a scan, the procedure is repeated, starting from the previously-scanned row, until the target fluence is applied.

3.3. Beam-Based Irradiation

Continuous monitoring of the beam parameters during the irradiation procedure enables to define beam-based (and other) *events*, to which the irradiation routine can react. An event is either active or inactive and is checked for at the beginning of each row as shown in fig. 5. In the case of one or more active events, the scan routine is halted while the beam remains on the shield, not irradiating the DUT, until all events are inactive. Typical events check for stable as well as sufficient beam current, a centered beam position but also adequately-low DUT temperature. Events becoming active while scanning a row are recorded and their effect on the fluence distribution can be accounted or even corrected for as shown in fig. 6. Here, due to a drop in beam current while traversing the DUT, a row was re-scanned post-irradiation with adjusted parameters to level the fluence distribution. This minimizes exposing the DUT to deficient beam conditions, maximizing the uniformity of the applied fluence.

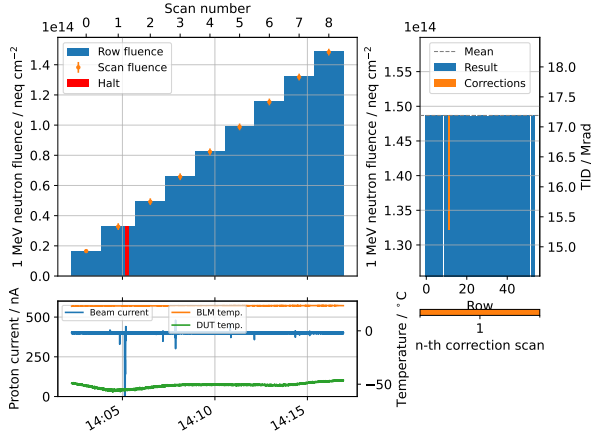


Figure 6: Overview of fluence per row and scan (top), beam current and temperatures (bottom) and the resulting fluence distribution (right).

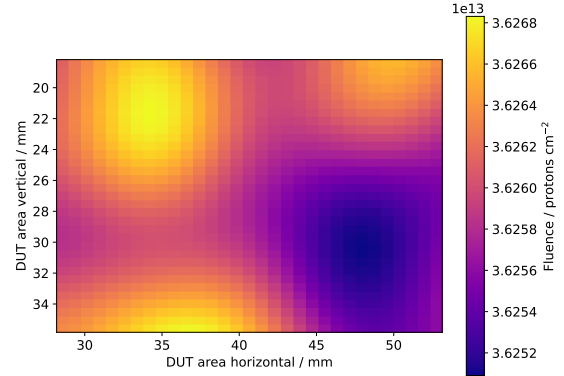


Figure 7: 2D fluence distribution on the DUT area, generated from the data recorded during irradiation. With a fluence of $3.6 \times 10^{13} \pm 4.4 \times 10^9$ p/cm², the relative standard deviation is $\ll 1\%$.

4. Dosimetry

4.1. Foil Activation Method

Conventionally, the determination of the primary particle fluence is performed via activation of metallic foils [5]. Here, depending on the ion species as well as energy, metals with an adequate isotope X of known production cross section Ω_X are selected and irradiated alongside the DUT within the uniform area indicated in fig. 5. After measurement of the resulting activity A_X , the particle fluence is a function of

$$\Phi(\Omega_X, A_X, M_{\text{foil}}, m_X, \lambda_X), \quad (2)$$

where M_{foil} is the foil mass, m_X the isotopes molar mass and λ_X its decay constant. The obtained fluence is a scalar value and the relative uncertainty typically in the order of $\Delta\Phi/\Phi \approx 10\%$ [5].

4.2. Beam-Based Methods

The continuous beam parameter monitoring allows for a purely beam-based, on- and offline dosimetry with a relative uncertainty of typically 2%, dominated by the beam current measurement. Following the procedure shown in fig. 5, the fluence applied within the uniform area per *complete scan* can be geometrically approximated as [5]

$$\Phi = \frac{I_{\text{beam}}}{z_{\text{ion}} \cdot q_e \cdot v_{\text{scan}} \cdot \Delta y}, \quad (3)$$

where I_{beam} is the ion beam current and Δy is the row separation. This allows for online monitoring

the fluence with row resolution, as shown in fig. 6. Here, corrections can be applied after identifying rows with insufficient fluence and re-irradiating them with adjusted parameters. Furthermore, the online fluence monitoring enables to pause the irradiation routine at any given fluence level to perform DUT measurements as well as applying custom fluence profiles.

Additionally, the data recorded during irradiation allows to generate a two-dimensional distribution of the particle fluence on the scan pattern as well as DUT area after irradiation. Here, the continuous monitoring of beam and setup parameters enables to interpolate the beam current along the paths of the irradiation routine. Assuming a Gaussian beam profile using the maximum estimations for the widths from the alignment process in section 1.1, a fluence distribution can be calculated for every point on the area by applying a Gaussian kernel. The resulting distribution on the DUT area is shown in fig. 7. With a relative standard deviation of $\ll 1\%$, the fluence can be assumed uniform within the uncertainties.

4.3. Comparison

To verify that the beam-based dosimetry methods via eq. (3) (M1) and irradiation data analysis (M2) as well as the dosimetry via foil activation (M3) yield comparable results, seven titanium foils were irradiated with (13.55 ± 0.05) MeV protons, corresponding to (12.22 ± 0.05) MeV on-foil, to fluences between 7×10^{13} p/cm² to 12×10^{14} p/cm². Here, the vanadium isotope ^{48}V is produced, via $^{48}\text{Ti} \xrightarrow{(p,n)} ^{48}\text{V}$, with a cross section of

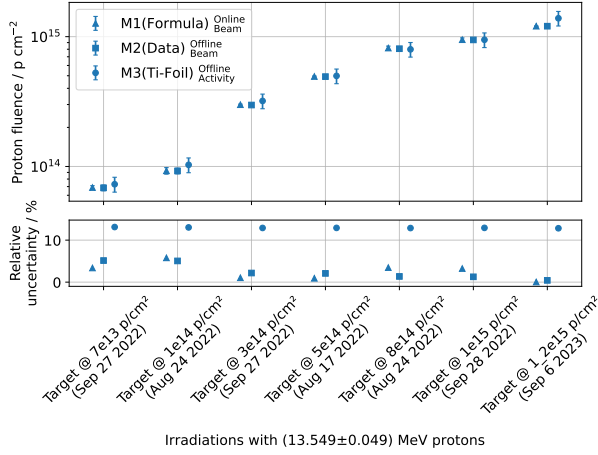


Figure 8: Comparison of dosimetry via beam-based methods (M1 & M2) and via foil activation (M3).

$\Omega_{48V} = (412 \pm 47)$ mb for (12.5 ± 0.2) MeV protons [6]. The resulting proton fluences as well as their relative uncertainties are shown in fig. 8. All methods yield consistent results whereas the beam-based approaches produce significantly lower, relative uncertainties of $\leq 5\%$ and additionally provide spatial resolution.

5. Proton Hardness Factor

5.1. Theory

The hardness factor κ is a scaling factor, representing a particles Non-Ionizing Energy Loss (NIEL) damage, normalized to 1 MeV neutron equivalents n_{eq} . It is given in MeV mb and depends on the particle species as well as energy, as depicted in fig. 9. For protons of 13.6 MeV, *GEANT4* [7] simulations displayed in fig. 10 yield an energy degradation to (12.28 ± 0.06) MeV when reaching the DUT's surface and (10.06 ± 0.11) MeV after 300 μm silicon. For these energies, a hardness factor of $\kappa_p \approx 4$ is expected. The NIEL hypothesis states that sensor properties such as leakage current scale linearly with the NIEL damage and therefore the particle fluence [8]. Here, the increase in leakage current ΔI_{leak} per depleted volume V is directly proportional to the fluence Φ

$$\frac{\Delta I_{leak}}{V} = \alpha \cdot \Phi, \quad (4)$$

where α is the *current-related damage factor* which itself is a function of annealing time and temperature. Conventionally, annealing is performed for 80 min at

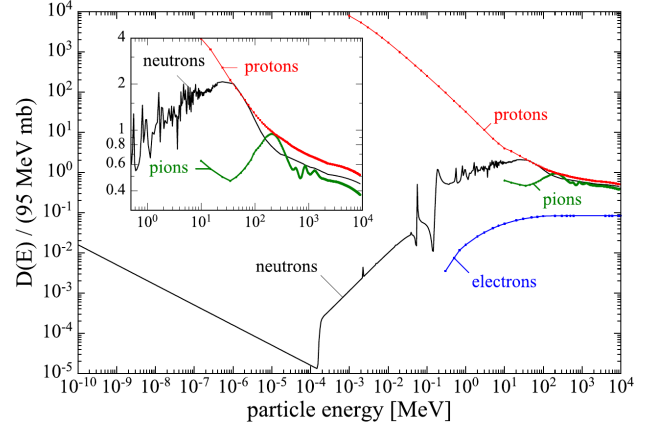


Figure 9: NIEL damage versus energy for various particles from [8]

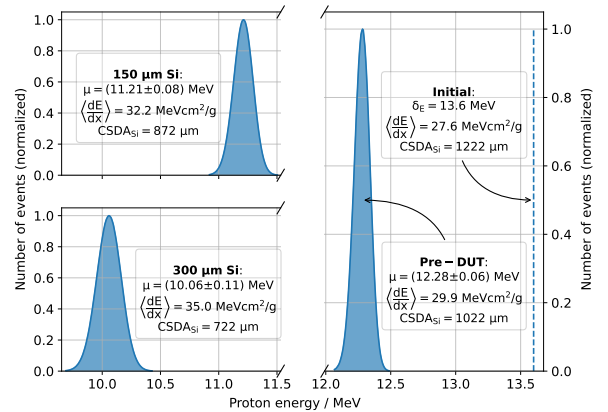


Figure 10: *GEANT4* simulation of initial, pre- and post-DUT proton energy distributions for two silicon thicknesses.

60 °C and leakage current measurements are performed at or scaled to 20 °C via [9]

$$I_{\text{leak}}(T) \propto T^2 \cdot \exp\left(-\frac{E_{\text{eff}}}{2k_B T}\right) \quad (5)$$

with $E_{\text{eff}} = (1.214 \pm 0.014) \text{ eV}$. Given the above conventions, $\alpha_{n_{\text{eq}}} = (3.99 \pm 0.03) \times 10^{-17} \text{ A cm}^{-1}$ for 1 MeV neutrons [8]. With knowledge of the current-related damage factor α_x for a given particle x , its hardness factor can be defined as

$$\kappa_x = \frac{\alpha_x}{\alpha_{n_{\text{eq}}}}. \quad (6)$$

5.2. Measurement

Using eqs. (4) and (6), the proton hardness factor is obtained by irradiation of sensors to different fluences as well as measurement of the leakage current at full depletion. Therefore, six 150 μm -thick, $(1.92 \times 0.96) \text{ cm}^2$, passive sensors from LFoundry were irradiated with $(13.52 \pm 0.04) \text{ MeV}$ protons to different fluences between $5 \times 10^{12} \text{ p/cm}^2$ to $16 \times 10^{13} \text{ p/cm}^2$ and electrically characterized. After irradiation, the sensors were annealed for 80 min at 60 °C and their leakage currents measured in a temperature-controlled environment between $-10 \text{ }^\circ\text{C}$ to $-25 \text{ }^\circ\text{C}$ with an error of 1 °C. Their IV behavior, scaled to 20 °C via eq. (5), pre- and post-irradiation is depicted in fig. 11. Using the method de-

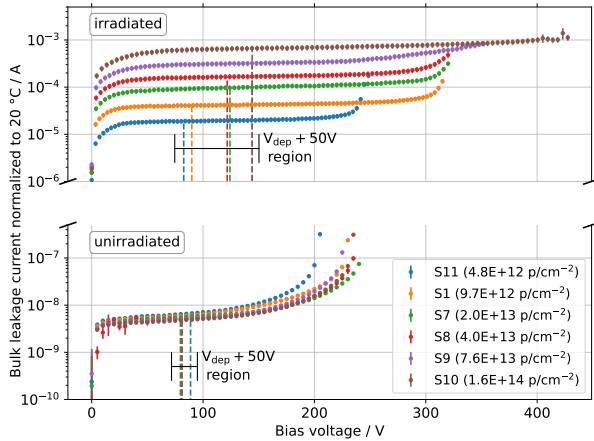


Figure 11: IV curves scaled to 20 °C of 150 μm thick sensors before and after irradiation. The full depletion voltage V_{dep} was determined by CV characterization as described in [10].

scribed in [10], the full depletion voltage V_{dep} after irradiation for each sensor is determined via CV measurements at different frequencies. The expected increase of

leakage current with fluence can be observed. The leakage current is evaluated at $V_{\text{dep}} + 50 \text{ V}$ to ensure full depletion where an uncertainty of 10 μm is assumed on the sensor thickness to account for processing variances. To obtain α_p , the increase in leakage current per depleted volume is plotted versus the respective proton fluence, as shown in fig. 12. A linear fit according to eq. (4) was performed and $\alpha_p = (1.48 \pm 0.04) \times 10^{-16} \text{ A cm}^{-1}$ was extracted which yields a proton hardness factor of

$$\kappa_p = \frac{\alpha_p}{\alpha_{n_{\text{eq}}}} = 3.71 \pm 0.11.$$

This is in agreement with the data shown in fig. 9 for the expected 12.3 MeV protons on the DUT, enabling irradiation of up to $10^{16} \text{ n}_{\text{eq}} \text{ cm}^{-2}$ within a few hours.

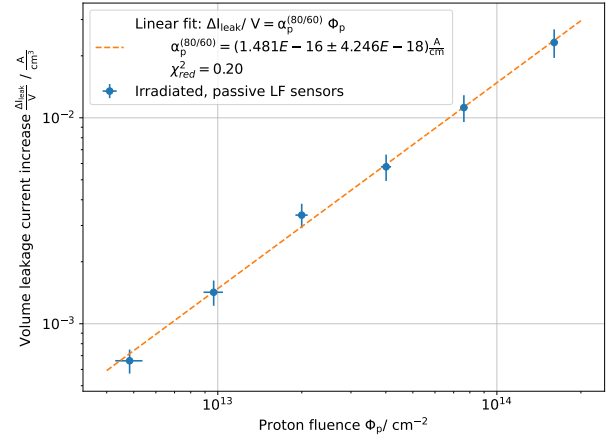


Figure 12: Leakage current increase per depleted volume versus applied proton fluence.

6. Limitations

The low proton energy of 12.3 MeV on the DUT constrains the NIEL scaling accuracy for thick silicon devices. As indicated in fig. 9, the hardness factor strongly depends on the proton energy in this regime. The energy loss due to ionization while traversing the DUT increases the hardness factor gradually. Here, for a silicon thickness of 300 μm , an energy loss of 2.2 MeV (see fig. 10) corresponds to an expected increase of the hardness factor of approximately 10% between entry and exit. Therefore, the stated proton hardness factor of $\kappa_p = 3.71 \pm 0.11$ is only accurate for DUTs $\leq 150 \mu\text{m}$ silicon and generally a thickness $\leq 300 \mu\text{m}$ is preferable. For thicker devices up to 300 μm , an increased hardness factor as well as uncertainty of $\kappa_p = 4.0 \pm 0.4$

is assumed, in accordance to the expected increase due to energy loss by ionization.

7. Conclusion

In this work, a modern proton irradiation site at the Bonn Isochronous Cyclotron (BIC) of Bonn University is described. DUTs are irradiated with 13.6 MeV protons inside a cool box at $\leq -20^\circ\text{C}$ which is moved through the stationary beam along a scan grid. Custom beam diagnostics facilitate online beam parameter monitoring at the extraction to the setup, enabling a beam-driven irradiation routine as well as a purely beam-based on- and offline dosimetry. Test irradiations of titanium foils verify that the beam-based and standard dosimetry via foil activation yield comparable results whereas the beam-based methods provide a lower uncertainty. Performing electrical characterization of thin sensors before and after irradiation allows to extract a proton hardness of $\kappa_p = 3.71 \pm 0.11$, in agreement with expectations. Due to the low proton energy at the BIC, DUTs with a thickness $\leq 300\ \mu\text{m}$ silicon are preferable to ensure accurate NIEL scaling.

References

- [1] D. Sauerland, P. Wolf, P.-D. Eversheim, R. Beck, J. Dingfelder, Proton irradiation site for si-detectors at the bonn isochronous cyclotron, in: 13th Int. Particle Acc. Conf., no. 13 in International Particle Accelerator Conference, JACoW Publishing, 2022, pp. 130–132. doi:10.18429/JACoW-IPAC2022-MOPOST030. URL <https://ipac2022.vrws.de/papers/mopost030.pdf>
- [2] H. Garnir, P. Dumont, Y. Baudinet-Robinet, Secondary electron emission from thin foils under fast ion bombardment, Nuclear Instruments and Methods in Physics Research 202 (1) (1982) 187–192. doi:[https://doi.org/10.1016/0167-5087\(82\)90394-5](https://doi.org/10.1016/0167-5087(82)90394-5). URL <https://www.sciencedirect.com/science/article/pii/0167508782903945>
- [3] C. Peterson, R. Laubert, Carbon accumulation on target surfaces irradiated by protons, IEEE Transactions on Nuclear Science 24 (3) (1977) 1542–1544. doi:10.1109/TNS.1977.4329004.
- [4] D. Sauerland, P. Wolf, P.-D. Eversheim, R. Beck, J. Dingfelder, Proton irradiation site for high-uniformity radiation hardness tests of silicon detectors at the bonn isochronous cyclotron, in: 23rd Int. Conf. on Cyclotrons and their Applications, no. 23 in International Conference on Cyclotron and their Applications, JACoW Publishing, 2022, pp. 130–132. doi:10.18429/JACoW-IPAC2022-MOPOST030. URL <https://ipac2022.vrws.de/papers/mopost030.pdf>
- [5] Dierlamm, Alexander, Irradiations in Karlsruhe, talk given on 16th RD50 workshop in Barcelona, Spain (06 2010). URL <https://indico.cern.ch/event/86625/contributions/2103519/>
- [6] F. Szelecsényi, F. Tárkányi, S. Takács, A. Hermanne, M. Sonck, Y. Shubin, M. Mustafa, Z. Youxiang, Excitation function for the natti(p,x)48v nuclear process: Evaluation and new measurements for practical applications, Nuclear Instruments and Methods in Physics Research Section B: Beam Interactions with Materials and Atoms 174 (2001) 47–64. doi:10.1016/S0168-583X(00)00516-4.
- [7] S. Agostinelli, et al., Geant4—a simulation toolkit, Nuclear Instruments and Methods in Physics Research Section A: Accelerators, Spectrometers, Detectors and Associated Equipment 506 (3) (2003) 250–303. doi:[https://doi.org/10.1016/S0168-9002\(03\)01368-8](https://doi.org/10.1016/S0168-9002(03)01368-8). URL <https://www.sciencedirect.com/science/article/pii/S0168900203013688>
- [8] M. Moll, Displacement damage in silicon detectors for high energy physics, IEEE Transactions on Nuclear Science 65 (8) (2018) 1561–1582. doi:10.1109/TNS.2018.2819506.
- [9] A. Chilingarov, Temperature dependence of the current generated in si bulk, Journal of Instrumentation 8 (2013) P10003–P10003. doi:10.1088/1748-0221/8/10/P10003.
- [10] Mägdefessel, Sven, Understanding the Frequency Dependence of CV Measurements of Irradiated Silicon Detectors, talk given on 41st RD50 workshop in Sevilla, Spain (11 2022). URL <https://indico.cern.ch/event/1132520/contributions/5140043/>